Journal of Magnetic Resonance **146,** 132–139 (2000)
doi:10.1006/jmre.2000.2128, available online at http://www.idealibrary.com on IDEAL®

Recoupling of Heteronuclear Dipolar Interactions with Rotational-Echo Double-Resonance at High Magic-Angle Spinning Frequencies

Christopher P. Jaroniec,* Brett A. Tounge,*,† Chad M. Rienstra,*,[1] Judith Herzfeld,† and Robert G. Griffin*,[2]

*Department of Chemistry and Francis Bitter Magnet Laboratory, Massachusetts Institute of Technology, Cambridge, Massachusetts 02139; and †Department of Chemistry, Brandeis University, Waltham, Massachusetts 02254

Received February 2, 2000; revised May 22, 2000

Heteronuclear dipolar recoupling with rotational-echo double-resonance (REDOR) is investigated in the rapid magic-angle spinning regime, where radiofrequency irradiation occupies a significant fraction of the rotor period (10–60%). We demonstrate, in two model ^{13}C–^{15}N spin systems, [1-^{13}C, ^{15}N] and [2-^{13}C, ^{15}N]glycine, that REDOR $\Delta S/S_0$ curves acquired at high MAS rates and relatively low recoupling fields are nearly identical to the $\Delta S/S_0$ curve expected for REDOR with ideal δ-function pulses. The only noticeable effect of the finite π pulse length on the recoupling is a minor scaling of the dipolar oscillation frequency. Experimental results are explained using both numerical calculations and average Hamiltonian theory, which is used to derive analytical expressions for evolution under REDOR recoupling sequences with different π pulse phasing schemes. For *xy*-4 and extensions thereof, finite pulses scale only the dipolar oscillation frequency by a well-defined factor. For other phasing schemes (e.g., *xx*-4 and *x*$\bar{x}$-4) both the frequency and amplitude of the oscillation are expected to change. © 2000 Academic Press

Key Words: **solid-state NMR; magic-angle spinning; heteronuclear dipolar recoupling; rotational-echo double-resonance; finite pulse effects.**

INTRODUCTION

Distance and dihedral angle constraints are powerful means for characterizing the three-dimensional structure of biomolecules. In solution-state NMR, the use of the nuclear Overhauser effect to establish through-space connectivities between ^1H nuclei is the foundation of structural studies of proteins and nucleic acids (*1*). In addition, recently developed experiments (*2, 3*) can be used to correlate anisotropic interactions and provide direct information about dihedral angles. In magic-angle spinning (MAS) solid-state NMR, homo- and heteronuclear dipolar recoupling techniques (*4–8*) are employed to measure internuclear distances and relative orientations of dipolar tensors.

The rotational-echo double resonance (REDOR) pulse sequence (*9, 10*) is frequently used to recouple heteronuclear dipolar interactions in isolated pairs of spin-$\frac{1}{2}$ nuclei, usually at relatively low magic-angle spinning frequencies ($\omega_r/2\pi \sim$ 2–8 kHz). REDOR is well compensated for pulse imperfections and resonance offsets (*11*) when recoupling π pulses are phased according to schemes based on *xy*-4 (*12*), and the technique has been successfully applied to many systems of biological interest (*13–17*).

REDOR experiments in spin systems involving multiple low-γ nuclei (*18–21*) and/or strong ^1H couplings (*22*) can potentially benefit from spinning frequencies in the regime $\omega_r/2\pi \sim$ 10–30 kHz. However, a concern in relation to the performance of REDOR at high MAS frequencies is the effect of the finite π pulse length on the recoupling (*23, 24*). The major aim of the work presented here is to investigate the REDOR recoupling dynamics under conditions where a significant fraction of the rotor period is occupied by RF pulses.

THEORY

The effect of finite pulses on the REDOR (Fig. 1) dipolar dephasing curve has been considered previously using Floquet theory (*25, 26*) and average Hamiltonian theory (AHT) (*23*). Here we derive analytical expressions for the first-order average Hamiltonians (*27*) for REDOR sequences with finite pulse lengths and different π pulse phasing schemes. Calculations were performed for the following phasing schemes: (i) *xyxy* (REDOR *xy*-4), (ii) *xxxx* (REDOR *xx*-4), and (iii) *x*$\bar{x}$*x*$\bar{x}$ (REDOR *x*$\bar{x}$-4). Considering only the heteronuclear dipolar coupling and finite pulse lengths (i.e., neglecting resonance offsets, CSAs, and pulse imperfections such as RF inhomogeneity and phase transients), all phasing schemes derived from *xy*-4 (*12*) have the same first-order average Hamiltonian (in our experiments we have used the *xy*-16 scheme). REDOR *xx*-4 and REDOR *x*$\bar{x}$-4 simulations are included for comparison, although we have not performed experiments with these phasing schemes. In addition, for comparison with the analytical AHT results, we have carried out simulations for the different REDOR sequences by the stepwise numerical propagation of the density operator for a two-spin system.

[1] Present address: Department of Chemistry, Columbia University, New York, NY 10027.

[2] To whom correspondence should be addressed. E-mail: rgg@mit.edu. Fax: (617) 253-5405.

1090-7807/00 $35.00

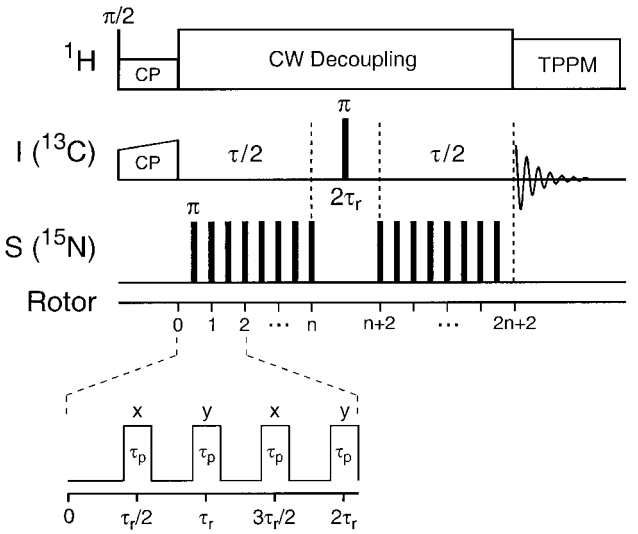

FIG. 1. REDOR pulse sequence (*9, 10*). Following ramped ^{1}H–^{13}C cross-polarization (*43*), the ^{13}C signal is observed as a spin-echo. The intensity of the echo is modulated due to the ^{13}C–^{15}N dipole interactions, recoupled by applying rotor-synchronized π pulses to ^{15}N spins. Timing of ^{15}N pulses within the rotor period is shown in the inset, and the basic *xy*-4 phase cycle is indicated. The experiments shown used the *xy*-16 scheme (*12*). The ^{13}C refocusing pulse was 10 μs and ^{15}N π pulses were 10–20 μs. Reference (S_0) experiments were performed in the absence of ^{15}N pulses.

The high-field truncated Hamiltonian for the heteronuclear dipolar coupling between spins I and S under magic-angle spinning can be expressed as (*28*)

$$H_{IS}(t) = -\frac{1}{2} b_{IS}\{\sin^2(\beta)\cos[2(\gamma + \omega_r t)] - \sqrt{2}\,\sin(2\beta)\cos(\gamma + \omega_r t)\}2I_zS_z, \quad [1]$$

where

$$b_{IS} = -\left(\frac{\mu_0}{4\pi}\right)\frac{\gamma_I\gamma_S\hbar}{r_{IS}^3} \quad [2]$$

is the dipolar coupling constant, which depends on the I–S distance, r_{IS}, and gyromagnetic ratios characteristic of the I and S spins, γ_I and γ_S, respectively. The Euler angles, β and γ, relate the I–S dipole vector to the rotor-fixed reference frame.

In the interaction representation defined by the RF field, the Hamiltonian for the I–S dipolar coupling acquires an additional time-dependence according to

$$\tilde{H}_{IS}(t) = U_{rf}^{-1}(t, t_0)\,H_{IS}(t)\,U_{rf}(t, t_0), \quad [3]$$

where the propagator due to the RF pulse on the S spin along the x axis of the rotating frame is defined as

$$U_{rf}(t_2, t_1) = \exp\{-i\omega_{rf}S_x(t_2 - t_1)\}. \quad [4]$$

For the different REDOR sequences considered here, the RF pulses applied to the S spin impart a time-dependence to the S_z operator, and the interaction frame Hamiltonian can be written (*25, 26*)

$$\tilde{H}_{IS}(t) = \omega_{IS}(t)\{f(t)2I_zS_z + g(t)2I_zS_x + h(t)2I_zS_y\}, \quad [5]$$

where $\omega_{IS}(t)$ is the crystallite-dependent dipolar oscillation frequency (cf. Eq. [1]), and the coefficients $f(t)$, $g(t)$, and $h(t)$ are as shown in Fig. 2. Here, $f(t)$ is identical for all π pulse phasing schemes and toggles between ± 1 during subsequent delays between pulses. Coefficients $g(t)$ and $h(t)$ are a direct consequence of the finite pulses: they can be non-zero only

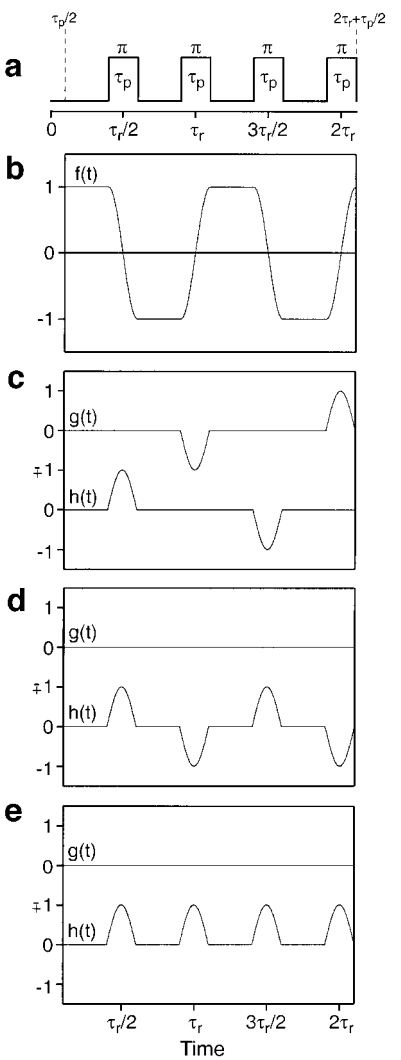

FIG. 2. (a) Details of the REDOR pulse sequence. (b–e) The $f(t)$, $g(t)$, and $h(t)$ coefficients in the interaction frame Hamiltonian (cf. Eq. [5]) for REDOR sequences with different phasing schemes. The $f(t)$ coefficient (b) is identical for all phasing schemes, and the $g(t)$ and $h(t)$ coefficients, shown for (c) REDOR *xy*-4, (d) REDOR *xx*-4, (e) and REDOR $x\bar{x}$-4, are different for the various phasing schemes.

during the pulses and are different for the various phasing schemes (*26*).

The first-order average Hamiltonian is calculated as the average of the interaction frame Hamiltonian over the cycle time, t_c, of the pulse sequence (*27*):

$$\overline{\tilde{H}}_{\mathrm{IS}}^{(1)} = \frac{1}{t_c}\int_{t_0}^{t_0+t_c} \tilde{H}_{\mathrm{IS}}(t)dt. \quad [6]$$

Explicit calculation of the first-order average Hamiltonian for the I–S dipolar coupling for REDOR *xy*-4 with finite pulses yields

$$\overline{\tilde{H}}_{\mathrm{IS}}^{(1)} = -\frac{\sqrt{2}}{\pi} b_{\mathrm{IS}} \frac{\cos((\pi/2)\varphi)}{1-\varphi^2} \sin(2\beta)\sin(\gamma)2I_zS_z, \quad [7]$$

where

$$\varphi = \frac{2\tau_p}{\tau_r} \quad [8]$$

is the fraction of the rotor period occupied by RF pulses, defined in the range $0 \leq \varphi \leq 1$. With the initial density operator $\rho(0) = I_x$, the evolution under the average Hamiltonian in Eq. [7] results in the observable signal for individual crystallites,

$$S(\tau) = \cos(\omega\tau), \quad [9]$$

with

$$\omega = -\frac{\sqrt{2}}{\pi} b_{\mathrm{IS}} \frac{\cos((\pi/2)\varphi)}{1-\varphi^2} \sin(2\beta)\sin(\gamma). \quad [10]$$

We note that the effective dipolar coupling constant, b_{IS}^{eff}, for REDOR *xy*-4 with finite pulses, differs from the dipolar coupling constant for the sequence with ideal δ-function pulses (i.e., $\varphi = 0$) only by the factor

$$\kappa \equiv \frac{b_{\mathrm{IS}}^{eff}}{b_{\mathrm{IS}}} = \frac{\cos((\pi/2)\varphi)}{1-\varphi^2}. \quad [11]$$

In the limit of windowless RF irradiation, we obtain $\lim_{\varphi\to 1}\kappa = \pi/4$. However, for relatively large values of φ, which are of practical interest, κ remains close to unity. For $\varphi = 0.6$ (e.g., $\omega_r/2\pi = 30$ kHz and $\omega_{rf}/2\pi = 50$ kHz) the effective dipolar coupling is expected to be only ~8% lower than the coupling in the $\varphi = 0$ limit.

Similar derivations of the first-order average Hamiltonian for REDOR *xx*-4 and REDOR $x\bar{x}$-4 yield

$$\overline{\tilde{H}}_{\mathrm{IS}}^{(1)} = -\frac{\sqrt{2}}{\pi} b_{\mathrm{IS}} \frac{\cos((\pi/2)\varphi)}{1-\varphi^2} \times \sin(2\beta)[\sin(\gamma)2I_zS_z + \varphi\cos(\gamma)2I_zS_y] \quad [12]$$

and

$$\overline{\tilde{H}}_{\mathrm{IS}}^{(1)} = -\frac{1}{\pi} b_{\mathrm{IS}}\left[\sqrt{2}\frac{\cos((\pi/2)\varphi)}{1-\varphi^2}\sin(2\beta)\sin(\gamma)2I_zS_z + \frac{\varphi\cos(\pi\varphi)}{1-4\varphi^2}\sin^2(\beta)\cos(2\gamma)2I_zS_y\right], \quad [13]$$

respectively.

For both sequences, the observable signal for individual crystallites is given by

$$S(\tau) = \cos(\sqrt{\Omega^2+\Phi^2}\tau), \quad [14]$$

with

$$\Omega_{xx} = \Omega_{x\bar{x}} = -\frac{\sqrt{2}}{\pi} b_{\mathrm{IS}} \frac{\cos((\pi/2)\varphi)}{1-\varphi^2} \sin(2\beta)\sin(\gamma), \quad [15a]$$

$$\Phi_{xx} = -\frac{\sqrt{2}}{\pi} b_{\mathrm{IS}} \frac{\varphi\cos((\pi/2)\varphi)}{1-\varphi^2} \sin(2\beta)\cos(\gamma), \quad [15b]$$

$$\Phi_{x\bar{x}} = -\frac{1}{\pi} b_{\mathrm{IS}} \frac{\varphi\cos(\pi\varphi)}{1-4\varphi^2} \sin^2(\beta)\cos(2\gamma). \quad [15c]$$

Note that for REDOR *xx*-4, in the special case of windowless RF irradiation of constant phase ($\varphi = 1$ in Eqs. [15a]–[15b]), the observable signal reduces to the expression independent of the Euler angle, γ, expected for $n = \pm 1$ rotary resonance recoupling (*29*),

$$S(\tau) = \cos(\tilde{\omega}\tau), \quad [16]$$

with

$$\tilde{\omega} = -\frac{1}{2\sqrt{2}} b_{\mathrm{IS}}\sin(2\beta). \quad [17]$$

In Fig. 3 we compare the analytical finite pulse AHT expressions (cf. Eqs. [9], [10] and [14], [15]) with numerical simulations. The REDOR $(S_0 - S)/S_0 = \Delta S/S_0$ curves (S_0 and S represent the reference and dipolar dephasing experiments, respectively) were calculated for $b_{\mathrm{IS}} = 190$ Hz (corresponding to a C–N distance of 2.53 Å) and $\varphi = 0.1$–0.66. Excellent agreement is obtained between the first-order average Hamiltonian analysis and the numerical simulations for all phasing schemes considered. For REDOR *xy*-4 (Fig. 3a), the dipolar coupling is scaled from that expected for the ideal

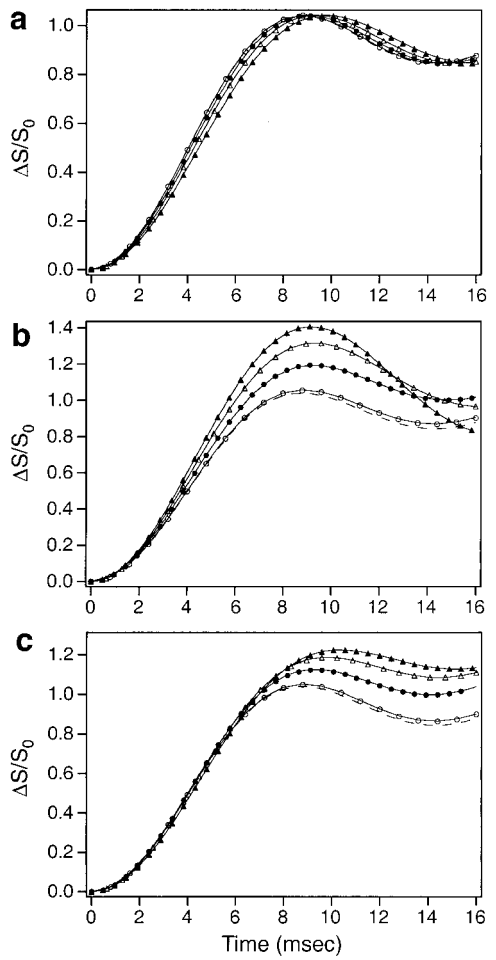

FIG. 3. Comparison of REDOR $\Delta S/S_0$ curves calculated numerically and using the average Hamiltonian expressions (see text) for $b_{IS} = 190$ Hz and different values of φ for (a) REDOR xy-4, (b) REDOR xx-4, and (c) REDOR $x\bar{x}$-4. Average Hamiltonian calculations are shown as discrete points for $\varphi = 0.1$ (○), 0.33 (●), 0.5 (△), and 0.66 (▲). Numerical simulations for the corresponding combination of φ and phasing scheme are shown as solid lines (- - -). For reference we also show the $\Delta S/S_0$ curve calculated for the ideal δ-function pulse sequence (- - -).

δ-function pulse sequence by a well-defined factor (cf. Eq. [11]). However, the amplitude of the oscillation remains unchanged. The effect of finite pulses on the dipolar coupling for REDOR xx-4 (Fig. 3b) and REDOR $x\bar{x}$-4 (Fig. 3c) is more complicated; for these sequences both the dipolar oscillation frequency and the amplitude are expected to change under conditions where the recoupling pulses occupy a significant fraction of the rotor period.

RESULTS AND DISCUSSION

In Figs. 4a and 4b we show experimental REDOR $\Delta S/S_0$ curves and simulations for [1-^{13}C, ^{15}N]glycine ($b_{IS} \sim 200$ Hz) and [2-^{13}C, ^{15}N]glycine ($b_{IS} \sim 900$ Hz), respectively, recorded at spinning frequencies $\omega_r/2\pi = 5$–15 kHz and recoupling RF fields $\omega_{rf}/2\pi = 25$–50 kHz (i.e., $0.1 \leq \varphi \leq 0.606$). The lower fields were used to create experimental conditions, where RF pulses occupy a significant fraction of the rotor period. For clarity, only a few representative $\Delta S/S_0$ curves are shown in Fig. 4. According to the simulations for REDOR xy-4 (cf. Fig. 3a), the finite π pulses are expected to scale the dipolar coupling by the factor κ given in Eq. [11]. As already noted, for most experimental conditions of practical interest we anticipate only a minor (i.e., <10%) decrease in b_{IS}. The scaling of the dipolar coupling can be observed experimentally in both model compounds considered here. In Fig. 4 we show that an increase in φ from 0.1 to 0.6 results in a relatively small decrease in the dipolar oscillation frequency.

For a more quantitative comparison of the average Hamiltonian result of Eq. [11] and experimental measurements of b_{IS}^{eff}, we fit the REDOR $\Delta S/S_0$ curves with the analytical expression

$$\langle \Delta S/S_0 \rangle(\tau) = \lambda \left[1 - \int_0^{\pi} d\beta \, \sin(\beta) \int_0^{2\pi} d\gamma \times \cos\left\{ -\frac{\sqrt{2}}{\pi} b_{IS}^{eff} \sin(2\beta)\sin(\gamma)\tau \right\} \right]. \quad [18]$$

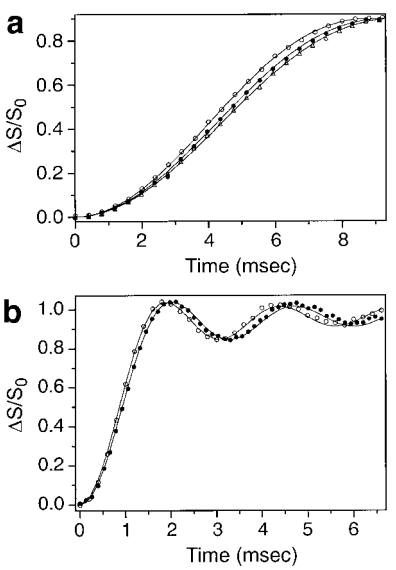

FIG. 4. Experimental REDOR $\Delta S/S_0$ curves for (a) [1-^{13}C, ^{15}N]glycine and (b) [2-^{13}C, ^{15}N]glycine. In (a) $\Delta S/S_0$ curves are shown for $\varphi = 0.1$ (○), 0.455 (●), and 0.606 (△), and in (b) curves are shown for $\varphi = 0.2$ (○) and 0.606 (●). The $\Delta S/S_0$ curves simulated according to Eq. [18] (see text) are also shown (—). All experiments were performed at 500.1 MHz ^{1}H frequency, $\omega_r/2\pi = 5$–15 kHz, and $\omega_{rf}(^{15}\text{N})/2\pi = 25$–50 kHz. During REDOR, CW ^{1}H decoupling was applied at 100 kHz (a) and 83 kHz (b). In all experiments 83 kHz TPPM ^{1}H decoupling (*34*) (phase difference $\phi = 12°$, $\tau = 5.3$ μs) was used during detection. For [1-^{13}C, ^{15}N]glycine, the REDOR period was incremented in steps of 0.4 ms ($\varphi = 0.1$, 0.2) and 0.396 ms ($\varphi = 0.303$, 0.455, 0.606). For [2-^{13}C, ^{15}N]glycine, the increments were 0.4 ms ($\varphi = 0.1$), 0.2 ms ($\varphi = 0.2$), and 0.132 ms ($\varphi = 0.303$, 0.455, 0.606).

TABLE 1
Experimentally Determined Effective C′–N and C^{α}–N Dipolar Couplings in Glycine

τ_p (μs)	τ_r (μs)	φ	b_{IS}^{eff}(C′-N) (Hz)	b_{IS}^{eff}(C^{α}-N) (Hz)
10	200	0.100	189 ± 2[a]	869 ± 35[a]
10	100	0.200	188 ± 2	886 ± 10
10	66	0.303	178 ± 5	875 ± 11
15	66	0.455	179 ± 2	854 ± 12
20	66	0.606	173 ± 2	826 ± 20

[a] Uncertainties in b_{IS}^{eff} (reported at 95% confidence level) were obtained following standard procedures described in Ref. (*30*).

Here, the scaling factor λ accounts for the contribution to the S_0 curve from ^{13}C spins without a neighboring ^{15}N (a result of dilution in natural abundance material and/or imperfect isotopic labeling). The incorporation of ^{13}C and ^{15}N labels in [1-^{13}C, ^{15}N] and [2-^{13}C, ^{15}N]glycine (Cambridge Isotope Laboratories) was ~98–99%. The [2-^{13}C, ^{15}N]glycine sample was not diluted in natural abundance glycine, and experimental data were best fit with $\lambda = 1.0$. The [1-^{13}C, ^{15}N]glycine was diluted with a ratio of ~1:10 in natural abundance glycine. With ±1% uncertainties in the dilution and ^{13}C and ^{15}N labeling, we expect $\lambda \sim 0.85$–0.90. For the REDOR experiment with $\varphi = 0.1$, the best fit was obtained for $\lambda = 0.865$, which was fixed at this value for all subsequent simulations.

For each experiment the effective dipolar coupling, b_{IS}^{eff}, was determined by minimizing the reduced χ^2 (*30*),

$$\chi_\nu^2 = \frac{1}{\nu}\sum_{i=1}^{n}\frac{1}{\sigma_i^2}[s_{exp}^i - s_{sim}^i]^2, \qquad [19]$$

where s_{exp}^i and s_{sim}^i are the intensities of the ith experimental and simulated points, respectively, σ_i^2 is the variance of the ith experimental point, and ν is the number of degrees of freedom defined as the difference between the number of experimental points in the $\Delta S/S_0$ curve, n, and the number of adjustable parameters used in the fit. In our simulations b_{IS}^{eff} was the only adjustable parameter (i.e., $\nu = n - 1$), and for each φ, σ_i^2 were obtained according to

$$\sigma_i^2 = \frac{1}{N-1}\sum_{j=1}^{N}\{[s_{exp}^i]_j - \overline{s_{exp}^i}\}^2. \qquad [20]$$

Here, N is the number of independently recorded $\Delta S/S_0$ curves ($N = 3$–9 in our experiments), $[s_{exp}^i]_j$ is the intensity of the ith experimental point, s_{exp}^i, in the jth $\Delta S/S_0$ curve, and $\overline{s_{exp}^i}$ is the average of N determinations of s_{exp}^i.

The resulting values of the effective dipolar coupling constants for [1-^{13}C, ^{15}N] and [2-^{13}C, ^{15}N]glycine are listed in Table 1. The b_{IS}^{eff} values were fit with the analytical AHT expression, describing the scaling of the dipolar coupling due to the finite pulses:

$$b_{IS}^{eff} = b_{IS}\frac{\cos((\pi/2)\varphi)}{1-\varphi^2}. \qquad [21]$$

The fitting was performed by minimizing χ_ν^2 (cf. Eq. [19]), where the single fit parameter was b_{IS}, the dipolar coupling in the limit of ideal δ-function pulses. For both model compounds all experimentally determined effective dipolar couplings are within 10% of the coupling in the $\varphi = 0$ limit, and the agreement between AHT calculations and experimental results shown in Fig. 5 is good. Therefore, for REDOR experiments where RF pulses occupy a significant fraction of the rotor period, the dipolar coupling constant, b_{IS}, can be calculated from the experimentally determined effective coupling as $b_{IS} = b_{IS}^{eff}(1-\varphi^2)/\cos((\pi/2)\varphi)$.

For the strong ^{13}C–^{15}N coupling in [2-^{13}C, ^{15}N]glycine, only the $\varphi = 0.1$ experiment ($\omega_r/2\pi = 5.0$ kHz, $\omega_{rf}/2\pi = 50$ kHz) deviates slightly from theory. However, for $\omega_r/2\pi \leq 5.0$ kHz we expect the accuracy and precision of the fit for the strong dipolar coupling to be somewhat compromised, due to the limitation in the number of points that can be acquired on the $\Delta S/S_0$ curve. In our experiments, the minimum increment for the REDOR period is $2\tau_r$ (i.e., only 18 data points could be acquired for 6.8 ms of dipolar evolution at $\omega_r/2\pi = 5.0$ kHz).

For the weaker ^{13}C–^{15}N coupling in [1-^{13}C, ^{15}N]glycine, all

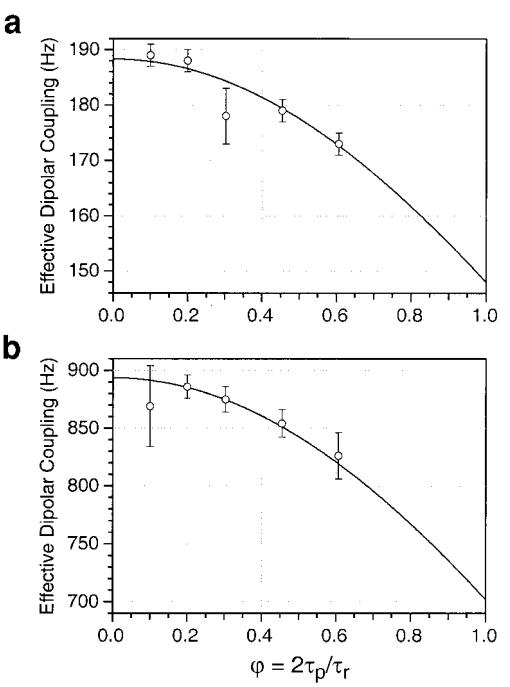

FIG. 5. Comparison of experimentally determined effective dipolar couplings (○) and the best-fit theoretical b_{IS}^{eff} vs φ curves (—) calculated using Eq. [21] for (a) [1-^{13}C, ^{15}N]glycine with $b_{IS} = 188$ Hz and (b) [2-^{13}C, ^{15}N]glycine with $b_{IS} = 894$ Hz.

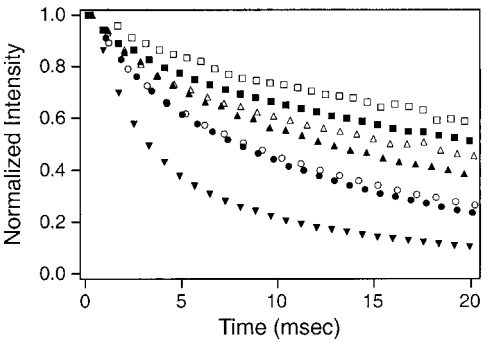

FIG. 6. Experimental REDOR S_0 curves for the C^α resonance in [1,2-^{13}C, ^{15}N]glycine, recorded at 750.0 MHz ^{1}H frequency. The S_0 curves were recorded by replacing the nonselective ^{13}C refocusing π pulse with a rotor-synchronized frequency-selective Gaussian π pulse, to remove coherent evolution under C′–C^α J coupling (*21*). The Gaussian pulses were ~200–300 μs (the exact pulse length was adjusted to occupy an even number of rotor periods) and 125 kHz CW ^{1}H decoupling was applied for the duration of the Gaussian pulse. During the indirect dimension and signal acquisition, 125 kHz TPPM ^{1}H decoupling (phase difference ϕ = 10–18°, τ = 3.6–3.7 μs) was used at spinning frequencies of 7.576 (●), 10.0 (○), 11.905 (▲), 13.889 (△), 15.152 (■), and 16.667 kHz (□). TPPM decoupling was optimized for each spinning frequency by minimizing the C^α linewidth in the direct dimension. For comparison we also show the S_0 curve at 15.152 kHz MAS and 125 kHz CW ^{1}H decoupling (▼).

experimental points, except $\varphi = 0.303$, agree well with theory. The effective C′–N dipolar coupling for $\varphi = 0.303$ was determined to be $b_{IS}^{eff} = 178 \pm 5$ Hz (note that the uncertainty in the value of b_{IS}^{eff} for this φ is significantly higher than the uncertainties for other φ given in Table 1). Careful inspection of the experimental data (not shown) revealed that points between ~7 and 9 ms of the $\varphi = 0.303$ $\Delta S/S_0$ curve reproducibly had ~2–3% lower intensity than expected for the simple model of C–N dipolar evolution described by Eq. [18], resulting in a worse fit (nine $\Delta S/S_0$ curves were recorded for these experimental conditions and all exhibited the same feature). We also note that for identical $\omega_r/2\pi$ and $\omega_{r_f}(^1H)/2\pi$, but different $\omega_{r_f}(^{15}N)/2\pi$ (i.e., $\varphi = 0.455$ and 0.606 experiments), $\Delta S/S_0$ curves could be fit very well to Eq. [18]. Therefore, the somewhat anomalous appearance of the $\varphi = 0.303$ $\Delta S/S_0$ curve may be related to a particularly unfavorable mismatch between the ^{15}N recoupling and ^{1}H decoupling RF fields under these experimental conditions (*31–33*).

As an example of the potential impact of higher spinning frequencies on REDOR experiments, in Fig. 6 we compare REDOR reference (S_0) curves for the C^α resonance in [1,2-^{13}C, ^{15}N]glycine recorded at $\omega_r/2\pi$ = 7.576–16.667 kHz, where the coherent evolution under the C′–C^α J coupling was removed as described previously (*21*). It is clear that for the CH_2 group in glycine the combination of fast MAS and two-pulse phase-modulated (TPPM) ^{1}H decoupling (*34*) significantly attenuates the dephasing of the ^{13}C spin-echo; the echo intensity at 20 ms of evolution increases from approximately 0.25 to 0.6 as the spinning frequency is increased from 7.576 to 16.667 kHz. In principle, the $\Delta S/S_0$ analysis should account for the rapid dephasing of the spin-echo. However, points on the $\Delta S/S_0$ curve will be defined with a higher signal-to-noise ratio when the echo-decay is attenuated, and this is of particular importance for REDOR data acquired for long evolution times (i.e., 20–30 ms). In systems for which no complications are introduced by rapid spinning, there do not appear to be any fundamental disadvantages to performing REDOR experiments at $\omega_r/2\pi$ ~ 10–30 kHz. The spin-echo intensity can be significantly higher under these conditions, while the recoupling performance is not appreciably affected (cf. Figs. 4 and 5).

The ^{13}C spin-echo intensity observed in the rapid spinning regime depends strongly on decoupling conditions, due to the ^{1}H reservoir becoming partially inhomogeneous (*35*). Specifically, at $\omega_r/2\pi \geq$ ~10 kHz CW ^{1}H decoupling deteriorates, while high-power TPPM decoupling effectively restores the echo intensity. In analogy to the line broadening observed in spectra of well-isolated spin pairs (*36–39*), the signal loss associated with CW decoupling can be described by the magnitude of the second-order cross-term between the ^{1}H chemical shielding and ^{13}C–^{1}H dipolar coupling tensors relative to the ^{1}H–^{1}H spin diffusion rate constant (*38, 39*). A particularly unfavorable situation for CW-decoupled spin systems can arise from the combination of high static magnetic fields, where the ^{1}H CSA magnitude increases, and very high MAS frequencies, for which the proton spin diffusion rate decreases and the tightly coupled spin system approaches an ensemble of isolated spin pairs (*39*). Under TPPM ^{1}H decoupling $(\tau_{-\phi/2}\tau_{+\phi/2})_n$, the magnitude of the second-order cross-term can be scaled down significantly by a proper choice of the phase difference, ϕ, leading to a decrease in the residual dipolar linewidth (*38*). In addition, Ernst *et al.* (*39*) have recently shown that the performance of high-power TPPM ^{1}H decoupling does not deteriorate at high static magnetic fields for spinning frequencies up to 30 kHz. Similar indications that the ^{1}H reservoir displays partially inhomogeneous behavior in CH_2 groups for spinning frequencies in the $\omega_r/2\pi$ ~ 15 kHz regime have been observed recently in rotating frame experiments (*40*).

The use of higher MAS frequencies for REDOR experiments on multiply ^{13}C labeled systems at high magnetic fields also offers some advantages. First, rapid spinning effectively attenuates residual ^{13}C–^{13}C dipolar couplings, which also contribute to the dephasing of the spin-echo (*20*). In addition, high rotation frequencies are required to avoid rotational resonance conditions (*41*), which can lead to severe line broadening in uniformly ^{13}C labeled samples. Finally, for ^{13}C spins with large CSA (e.g., carbonyl groups), fast spinning will result in an increased signal-to-noise ratio in the direct dimension, as the intensity of rotational sidebands is reduced (*35, 42*).

CONCLUSIONS

We have investigated the performance of the REDOR recoupling sequence in model ^{13}C–^{15}N spin systems under conditions where a significant fraction of the rotor period (10–

60%) is occupied by RF pulses. Experimental results were explained using numerical simulations and average Hamiltonian calculations. For *xy*-4 and related phasing schemes, the finite pulses were shown to have a minor effect on the dipolar scaling factor expected for REDOR with ideal δ-function pulses. Under most experimental conditions of practical interest, the dipolar scaling factor is reduced by only 1–5%; at relatively high spinning frequencies and weak RF fields the effect may be slightly larger ($\sim$5–10%). The changes in the dipolar scaling factor can be quantitatively described using the analytical expressions presented here, allowing for the accurate determination of the dipolar coupling. Therefore, we conclude that there appear to be no fundamental disadvantages to using REDOR recoupling at spinning frequencies in the $\omega_r/2\pi \sim$ 10–30 kHz regime. However, we would also like to note that since the primary aim of this work was to investigate the effect of finite RF pulses on the heteronuclear dipolar coupling, the model compounds selected represent favorable spin systems, with relatively weak ^{15}N–^{1}H dipolar couplings and negligible ^{15}N chemical-shielding anisotropy. In general, these interactions will be nonnegligible and can potentially influence REDOR dipolar dephasing curves. Investigations of these effects are currently in progress in our laboratory.

EXPERIMENTAL

Experiments were performed on custom-designed spectrometers operating at ^{1}H Larmor frequencies of 500.1 and 750.0 MHz. Custom-designed quadruple- (500.1 MHz) and triple-resonance (750.0 MHz) transmission line MAS probes were used, equipped with Chemagnetics spinner modules (4 and 3.2 mm for the 500.1 and 750.0 MHz probes, respectively). Samples were centerpacked in rotors and the spinning frequencies in the range $\omega_r/2\pi \sim$ 5–17 kHz (see text for details) were controlled to $\pm$5 Hz using spin rate controllers from Doty Scientific and Bruker. This spinning frequency stability was adequate for performing all experiments described, and active synchronization of RF pulses within the rotor cycle was not required.

The REDOR pulse sequence employed in the experiments is shown in Fig. 1. Ramped cross-polarization (*43*) was used to create the initial ^{13}C transverse magnetization. In the experiments carried out on the 500.1 MHz spectrometer, the ^{13}C refocusing pulse was 10 μs, and ^{15}N pulses were 10–20 μs and phased according to the *xy*-16 scheme (*12*). We have investigated the performance of *xy*-4, *xy*-8, and *xy*-16 on [1-^{13}C, ^{15}N]glycine (data not shown) and observed identical dipolar dephasing curves for all phasing schemes. CW ^{1}H decoupling ($\omega_{rf}/2\pi$ = 83–100 kHz) was applied during the REDOR period, and 83 kHz TPPM ^{1}H decoupling (*34*) (phase difference $\phi = 12°$, $\tau = 5.3$ μs) was used during the acquisition of the FID. The experiments on the 750.0 MHz spectrometer (cf. Fig. 6) were carried out with 125 kHz CW or TPPM ^{1}H decoupling during the indirect dimension and 125 kHz TPPM ^{1}H decoupling (phase difference ϕ = 10°–18°, τ = 3.6–3.7 μs) during signal acquisition. In all experiments the recycle delay was 3.0 s and 16 transients were acquired per time point. The experiments were repeated at least three times (with good reproducibility) and were subsequently averaged.

ACKNOWLEDGMENTS

We thank M. Hohwy for the FORTRAN subroutines used in the numerical simulations and acknowledge many helpful discussions with B. Reif and M. Hohwy. C.P.J. thanks the NSF for a Predoctoral Fellowship, B.A.T. thanks the American Cancer Society for a Postdoctoral Fellowship (PF-99-260-01-GMC), and C.M.R. thanks the Howard Hughes Medical Institute for a Predoctoral Fellowship. This research was also supported by NIH grants GM-23289, GM-36810, and RR-00995.

REFERENCES

1. K. Wüthrich, "NMR of Proteins and Nucleic Acids," Wiley, New York (1986).
2. B. Reif, M. Hennig, and C. Griesinger, Direct measurement of angles between bond vectors in high-resolution NMR, *Science* **276,** 1230–1233 (1997).
3. D. Yang, R. Konrat, and L. E. Kay, A multidimensional NMR experiment for measurement of the protein dihedral angle ψ based on cross-correlated relaxation between $^{1}H^{\alpha}$–$^{13}C^{\alpha}$ dipolar and $^{13}C'$ (carbonyl) chemical shift anisotropy mechanisms, *J. Am. Chem. Soc.* **119,** 11938–11940 (1997).
4. J. M. Griffiths and R. G. Griffin, Nuclear magnetic resonance methods for measuring dipolar couplings in rotating solids, *Anal. Chim. Acta* **283,** 1081–1101 (1993).
5. A. E. Bennett, R. G. Griffin, and S. Vega, Recoupling of homo- and heteronuclear dipolar interactions in rotating solids, *in* "Solid State NMR IV: Methods and Applications of Solid-State NMR" (B. Blumich, Ed.), pp. 1–77, Springer-Verlag, Berlin (1994).
6. L. M. McDowell and J. Schaefer, High-resolution NMR of biological solids, *Curr. Opinion Struct. Biol.* **6,** 624–629 (1996).
7. R. G. Griffin, Dipolar recoupling in MAS spectra of biological solids, *Nature Struct. Biol.* **5,** 508–512 (1998).
8. R. Fu and T. A. Cross, Solid-state nuclear magnetic resonance investigation of protein and polypeptide structure. *Annu. Rev. Biophys. Biomol. Struct.* **28,** 235–268 (1999).
9. T. Gullion and J. Schaefer, Rotational-echo double-resonance NMR, *J. Magn. Reson.* **81,** 196–200 (1989).
10. T. Gullion and J. Schaefer, Detection of weak heteronuclear dipolar coupling by rotational-echo double-resonance nuclear magnetic resonance, *Adv. Magn. Reson.* **13,** 57–83 (1989).
11. T. Gullion and J. Schaefer, Elimination of resonance offset effects in rotational-echo, double-resonance NMR, *J. Magn. Reson.* **92,** 439–442 (1991).
12. T. Gullion, D. B. Baker, and M. S. Conradi, New, compensated Carr–Purcell sequences, *J. Magn. Reson.* **89,** 479–484 (1990).
13. Y. Li, R. J. Appleyard, W. A. Shuttleworth, and J. N. S. Evans, Time-resolved solid-state REDOR NMR measurements on 5-enolpyruvylshikimate-3-phosphate synthase, *J. Am. Chem. Soc.* **116,** 10799–10800 (1994).
14. L. M. McDowell, A. Schmidt, E. R. Cohen, D. R. Studelska, and J. Schaefer, Structural constraints on the ternary complex of 5-enolpyruvylshikimate-3-phosphate synthase from rotational-echo double-resonance NMR, *J. Mol. Biol.* **256,** 160–171 (1996).

15. K. Nishimura, A. Naito, S. Tuzi, H. Saito, C. Hashimoto, and M. Aida, Determination of the three-dimensional structure of crystalline Leu-enkephalin based on six sets of accurately determined interatomic distances from ^{13}C-REDOR NMR and the conformation-dependent ^{13}C chemical shifts, *J. Phys. Chem. B* **102,** 7476–7483 (1998).
16. C. A. Michal and L. W. Jelinski, Rotational-echo double-resonance in complex biopolymers: A study of Nephila clavipes dragline silk, *J. Biomol. NMR* **12,** 231–241 (1998).
17. M. E. Merritt, S. Th. Sigurdsson, and G. P. Drobny, Long-range distance measurements to the phosphodiester backbone of solid nucleic acids using ^{31}P–^{19}F REDOR NMR, *J. Am. Chem. Soc.* **121,** 6070–6071 (1999).
18. C. A. Michal and L. W. Jelinski, REDOR 3D: Heteronuclear distance measurements in uniformly labeled and natural abundance solids, *J. Am. Chem. Soc.* **119,** 9059–9060 (1997).
19. T. Gullion and C. H. Pennington, θ-REDOR: An MAS NMR method to simplify multiple coupled heteronuclear spin systems, *Chem. Phys. Lett.* **290,** 88–93 (1998).
20. J. Schaefer, REDOR-determined distances from heterospins to clusters of ^{13}C labels, *J. Magn. Reson.* **137,** 272–275 (1999).
21. C. P. Jaroniec, B. A. Tounge, C. M. Rienstra, J. Herzfeld, and R. G. Griffin, Measurement of ^{13}C–^{15}N distances in uniformly ^{13}C labeled biomolecules: J-decoupled REDOR, *J. Am. Chem. Soc.* **121,** 10237–10238 (1999).
22. K. Saalwächter, R. Graf, and H. W. Spiess, Recoupled polarization transfer ^{1}H–^{13}C multiple-quantum correlation in solids under ultrafast MAS, *J. Magn. Reson.* **140,** 471–476 (1999).
23. A. Naito, K. Nishimura, S. Kimura, S. Tuzi, M. Aida, N. Yasuoka, and H. Saito, Determination of the three-dimensional structure of a new crystalline form of N-acetyl-Pro-Gly-Phe as revealed by ^{13}C REDOR, X-ray diffraction, and molecular dynamics simulation, *J. Phys. Chem.* **100,** 14995–15004 (1996); A. Naito, S. Tuzi, and H. Saito, Dipolar interactions and interatomic distances, *in* "Solid State NMR of Polymers" (I. Ando and T. Asakura, Eds.), pp. 23–49, Elsevier, Amsterdam (1998).
24. R. Fu, S. A. Smith, and G. Bodenhausen, Recoupling of heteronuclear dipolar interactions in solid-state magic-angle spinning NMR by simultaneous frequency and amplitude modulation, *Chem. Phys. Lett.* **272,** 361–369 (1997).
25. A. Schmidt and S. Vega, The transition amplitudes of centerband and sidebands in NMR spectra of rotating solids, *Isr. J. Chem.* **32,** 215–230 (1992).
26. O. Weintraub and S. Vega, Floquet density matrices and effective Hamiltonians in magic-angle-spinning NMR spectroscopy, *J. Magn. Reson. A* **105,** 245–267 (1993).
27. U. Haeberlen and J. S. Waugh, Coherent averaging effects in magnetic resonance, *Phys. Rev.* **175,** 453–467 (1968).
28. M. Mehring, "Principles of High Resolution NMR in Solids," Springer-Verlag, Berlin (1983).
29. T. G. Oas, R. G. Griffin, and M. H. Levitt, Rotary resonance recoupling of dipolar interactions in solid-state nuclear magnetic resonance spectroscopy, *J. Chem. Phys.* **89,** 692–695 (1988).
30. D. P. Shoemaker, C. W. Garland, and J. W. Nibler, "Experiments in Physical Chemistry," McGraw–Hill, New York (1989). [And references therein]
31. Y. Ishii, J. Ashida, and T. Terao, ^{13}C–^{1}H dipolar recoupling dynamics in ^{13}C multiple-pulse solid-state NMR, *Chem. Phys. Lett.* **246,** 439–445 (1995).
32. A. E. Bennett, "Dipolar Recoupling and Decoupling in Solid State Nuclear Magnetic Resonance Spectroscopy," Ph.D. Thesis, Massachusetts Institute of Technology (1995).
33. A. E. Bennett, C. M. Rienstra, J. M. Griffiths, W. Zhen, P. T. Lansbury, Jr., and R. G. Griffin, Homonuclear radio frequency-driven recoupling in rotating solids, *J. Chem. Phys.* **108,** 9463–9479 (1998).
34. A. E. Bennett, C. M. Rienstra, M. Auger, K. V. Lakshmi, and R. G. Griffin, Heteronuclear decoupling in rotating solids, *J. Chem. Phys.* **103,** 6951–6957 (1995).
35. M. M. Maricq and J. S. Waugh, NMR in rotating solids, *J. Chem. Phys.* **70,** 3300–3316 (1979).
36. I. J. Shannon, K. D. M. Harris, and S. Arumugam, High-resolution solid-state ^{13}C NMR studies of ferrocene as a function of magic angle sample spinning frequency, *Chem. Phys. Lett.* **196,** 588–594 (1992).
37. P. Tekely, P. Palmas, and D. Canet, Effect of proton spin exchange on the residual ^{13}C MAS NMR linewidths. Phase-modulated irradiation for efficient heteronuclear decoupling in rapidly rotating solids, *J. Magn. Reson. A* **107,** 129–133 (1994).
38. M. Ernst, S. Bush, A. C. Kolbert, and A. Pines, Second-order recoupling of chemical-shielding and dipolar-coupling tensors under spin decoupling in solid-state NMR, *J. Chem. Phys.* **105,** 3387–3397 (1996).
39. M. Ernst, H. Zimmermann, and B. H. Meier, A simple model for heteronuclear spin decoupling in solid-state NMR, *Chem. Phys. Lett.* **317,** 581–588 (2000).
40. M. Hohwy, C. M. Rienstra, C. P. Jaroniec, and R. G. Griffin, Fivefold symmetric homonuclear dipolar recoupling in rotating solids: Application to double quantum spectroscopy, *J. Chem. Phys.* **110,** 7983–7992 (1999).
41. D. P. Raleigh, M. H. Levitt, and R. G. Griffin, Rotational resonance in solid state NMR, *Chem. Phys. Lett.* **146,** 71–76 (1988).
42. J. Herzfeld and A. E. Berger, Sideband intensities in NMR spectra of samples spinning at the magic angle, *J. Chem. Phys.* **73,** 6021–6030 (1980).
43. G. Metz, X. Wu, and S. O. Smith, Ramped-amplitude cross-polarization in magic-angle-spinning NMR, *J. Magn. Reson. A* **110,** 219–227 (1994).